PTEP

Prog. Theor. Exp. Phys. **2020**, 043E01 (13 pages)
DOI: 10.1093/ptep/ptaa029

# Thermal state of transiently accreting neutron stars with additional heating beyond deep crustal heating

Helei Liu[1,*], Masa-aki Hashimoto[2], Guoliang Lü[1], Yasuhide Matsuo[3], Dehua Wen[4], and Tsuneo Noda[5]

[1]*School of Physical Science and Technology, Xinjiang University, Urumqi 830046, China*
[2]*Department of Physics, Kyushu University, Fukuoka 819-0395, Japan*
[3]*Nippo-cho, Minatokouhoku-ku, Yokohama, Kanagawa 223-0057, Japan*
[4]*School of Physics and Optoelectronic Technology, South China University of Technology, Guangzhou 510641, China*
[5]*Kurume Institute of Technology, Fukuoka 830-0052, Japan*
*E-mail: heleiliu@xju.edu.cn

Received January 16, 2020; Revised February 19, 2020; Accepted February 19, 2020; Published April 22, 2020

As some neutron star transients require an additional unknown heat source (referred to as "shallow heating") to explain their high temperatures at the beginning of quiescence, we investigate the effect of shallow heating as well as compressional heating on the thermal state of transiently accreting neutron stars with the use of evolutionary calculations in the present work. Through comparing our theoretical predictions of the equilibrium redshifted luminosities ($L_\gamma^\infty$) produced by both deep crustal heating and shallow heating/compressional heating for different time-averaged mass-accretion rates $\langle \dot{M} \rangle$ with 35 updated observations of soft X-ray transients, the results show that both shallow heating and compressional heating make significant contributions to the equilibrium redshifted luminosity. The hotter sources (XTE J1701, MAXI J0556, EXO 0748, Aql X-1 etc.) with higher accretion rates are more likely to be explained with the effect of shallow heating or compressional heating. In addition, for a proper shallow heat $q_{\rm sh}$ and mass-accretion rate $\dot{M}$, the effect of shallow heating could be simulated by compressional heating.

Subject Index E20, E25, E32, E34

## 1. Introduction

Neutron stars (NSs) are excellent laboratories for probing the nature of dense matter. One attractive avenue is to study the quiescent luminosity of transiently accreting NSs, for which the NSs reside in low-mass X-ray binaries (LMXBs) and accrete material onto their surfaces from their companions via Roche-lobe overflow. These systems are also called soft X-ray transients (SXTs) [1]. During the quiescent period (several years to decades), accretion halts or is strongly suppressed; the SXTs are in low quiescent luminosities ($L_{\rm q} \sim 10^{31–34}$ erg s$^{-1}$). During the X-ray burst period (several weeks to months), SXTs are at very high X-ray luminosities ($L_o > 10^{36–39}$ erg s$^{-1}$) due to the high mass-accretion rate. During this phase the continual compression of the crust induces a series of deep crustal heating events (electron capture, neutron emission, and pycnonuclear reactions) that

© The Author(s) 2020. Published by Oxford University Press on behalf of the Physical Society of Japan.
This is an Open Access article distributed under the terms of the Creative Commons Attribution License (http://creativecommons.org/licenses/by/4.0/), which permits unrestricted reuse, distribution, and reproduction in any medium, provided the original work is properly cited.

Downloaded from https://academic.oup.com/ptep/article/2020/4/043E01/5823818 by guest on 16 August 2022

releases 1–2 MeV per accreted nucleon [2–4]. Then, the crust is heated out of thermal equilibrium with the core. Once it turns to quiescence, thermal X-ray emission occurs from the surface of the NS so that the crust reaches equilibrium with the core again [5,6].

Yakovlev et al. first investigated the theoretical curves between quiescent luminosity and the average mass-accretion rate (also called the heating curve) by comparison with five observed SXTs [7]. Assuming the presence of the powerful direct Urca neutrino emission process, Beznogov and Yakovlev reasonably explained the 24 SXTs observed by Heinke et al. [8–12]. Also, Han and Steiner explored the heating curves by taking into account several variations (equation of state, superfluidity gaps, and so on) [13], Matsuo et al. investigated the quiescent luminosities of accreting neutron stars with the possibility of neutrino losses due to strong pion condensations in the evolutionary calculations [14]. Recently, there are 35 SXTs that have been cited in studying the quiescent luminosity of SXTs [15,16]. The above studies of the thermal states of transiently accreting neutron stars are in the quasi-stationary scenario (the crust and core are in thermal equilibrium during the observations at quiescence) where the thermal equilibrium is determined by the energy income due to deep crustal heating and the energy losses due to neutrino emission from the core and the crust and photon emission from the surface.

However, in about 10 SXTs, such as KS 1731-260, MXB 1659-29, and MAXI J0556-332, crustal cooling has been observed after outburst [1]. In order to fit their quiescent light curves, an additional energy source at a shallower depth in the neutron star crust (about 100–400 m from the surface, i.e., at lower densities: $\rho \sim 10^8$–$10^{10}$ g cm$^{-3}$) is needed. This heat source is called "shallow heating". The strength (amount and depth) of this shallow heating is uncertain. It can vary from one source to another or be different between outbursts in the same source. For example, KS 1731-260, MXB 1659-29, and Aql X-1 needed shallow heating of the order of $\sim$ 1–2 MeV nucleon$^{-1}$ [17–19], while MAXI J0556-332 required a strong shallow heating $\sim$ 6–17 MeV nucleon$^{-1}$ during outburst I, $\sim$ 2 MeV nucleon$^{-1}$ during outburst II, and $\sim$ 0.3 MeV nucleon$^{-1}$ during outburst III [20–22]. The physical origin of shallow heating is currently still unclear [21,23]. We note that Liu et al. fit the light curve of MAXI J0556-332 by nuclear energy generation due to the hot-CNO (carbon–nitrogen–oxygen) cycle in the envelope in addition to compressional heating and deep crustal heating with stellar evolutionary calculations [24].

Motivated by the shallow heating issue mentioned above, in this research, we explore the effect of additional heating such as shallow heating/compressional heating on the equilibrium state of SXTs. Although shallow heating may not exist in most of the SXTs, the equilibrium quiescent luminosities of crustal cooling sources (such as KS 1731-260, MXB 1659-29, MAXI J0556-332, Aql X-1 etc.) that need shallow heating have been estimated [15]; as a result, it is worthwhile to explore the effect of shallow heating on the thermal state of SXTs. On the other hand, compressional heating must be included in the stellar evolution [25]; the light curve of MAXI J0556-332 can be well explained with compressional heating rather than strong shallow heating [24], so we also plan to investigate the effect of compressional heating on the thermal state of SXTs.

The paper is structured as follows: in Sect. 2, we present the basic equations and input physics. In Sect. 3, we recall the quiescent luminosity of quasi-stationary SXTs in the evolutionary calculations, and compare the theoretical heating curves with the 35 updated SXTs. In Sect. 4, we study the effect of shallow heating/compressional heating on the quiescent emission of transiently accreting neutron stars. In Sect. 5, we give detailed discussions and an analysis, and in Sect. 6, we draw conclusions.



Downloaded from https://academic.oup.com/ptep/article/2020/4/043E01/5823818 by guest on 16 August 2022

## 2. Basic equations and physical inputs

In order to model the quiescent luminosity of transiently accreting neutron stars, we use the spherically symmetric stellar evolutionary calculations [25–27], which include full general relativistic effects formulated by Thorne [28]. Our model is based on the stellar evolutionary calculations of accreting neutron stars with neutrino cooling due to strong pion condensation [14]. We use the same basic equations and physics input as in Ref. [14]. Meanwhile, the physics inputs of shallow heating and compressional heating are described; we briefly summarize them below.

### *2.1. Basic equations of thermal evolution*

The structure and thermal evolution of spherically symmetric neutron stars in hydrostatic equilibrium are determined by differential equations as follows [28]:

$$\frac{\partial M_{tr}}{\partial r} = 4\pi r^2 \rho, \tag{1}$$

$$\frac{\partial P}{\partial r} = -\frac{GM_{tr}\rho}{r^2}\left(1+\frac{P}{\rho c^2}\right)\left(1+\frac{4\pi r^3 P}{M_{tr}c^2}\right) \times \left(1-\frac{2GM_{tr}}{rc^2}\right)^{-1}, \tag{2}$$

$$\frac{\partial (L_r e^{2\phi/c^2})}{\partial M_r} = e^{2\phi/c^2}(\varepsilon_n + \varepsilon_g - \varepsilon_\nu), \tag{3}$$

$$\frac{\partial \ln T}{\partial \ln P} = \nabla_{\rm rad}, \tag{4}$$

$$\frac{\partial M_{tr}}{\partial M_r} = \frac{\rho}{\rho_0}\left(1-\frac{2GM_{tr}}{rc^2}\right)^{1/2}, \tag{5}$$

$$\frac{\partial \phi}{\partial M_{tr}} = \frac{G(M_{tr}+4\pi r^3 P/c^2)}{4\pi r^4 \rho}\left(1-\frac{2GM_{tr}}{rc^2}\right)^{-1}, \tag{6}$$

where $M_{tr}$ and $M_r$ are the gravitational and rest masses inside a sphere of radius $r$, respectively; $\rho$ and $\rho_0$ are the total mass energy density and rest mass density, respectively; $T$ and $P$ are the local temperature and pressure, respectively; $\varepsilon_n$ and $\varepsilon_g$ denote the heating rate by nuclear burning and gravitational energy release, respectively; $\varepsilon_\nu$ is the energy loss rate by neutrino emission; $L_r$ is the local luminosity; $\nabla_{\rm rad}$ is the radiative temperature gradient, $\nabla_{\rm rad} = \frac{3}{16\pi acG}\frac{P}{T^4}\frac{\kappa L_r}{M_r}$, where $\kappa$ is opacity and is obtained by using the public codes [29,30] and $a$ is the Stefan–Boltzmann constant; $\phi$ is the gravitational potential. The above differential equations are solved with boundary conditions: $r = L_r = 0$ at $M_r = 0$, and $P = T = 0$ at $M_r = M$ in the presence of the equation of state.

We adopt the definition of mass fraction with changing mass $q = M_r/M(t)$, which is the most suitable method when the stellar mass ($M$) varies [31]. The gravitational energy released in Eq. (3), $\varepsilon_g$, is divided into two parts, i.e., $\varepsilon_g = \varepsilon_g^{(\rm h)} + \varepsilon_g^{(\rm nh)}$, where each part is described as follows [25]:

$$\varepsilon_g^{(\rm h)} = \exp\left(-\frac{\phi}{c^2}\right)\frac{\dot{M}}{M}\left(T\left.\frac{\partial s}{\partial \ln q}\right|_t + \mu_i\left.\frac{\partial N_i}{\partial \ln q}\right|_t\right), \tag{7}$$

$$\varepsilon_g^{(\rm nh)} = -\exp\left(-\frac{\phi}{c^2}\right)\left(T\left.\frac{\partial s}{\partial t}\right|_q + \mu_i\left.\frac{\partial N_i}{\partial t}\right|_q\right), \tag{8}$$



Downloaded from https://academic.oup.com/ptep/article/2020/4/043E01/5823818 by guest on 16 August 2022

**Table 1.** The central density $\rho_c$ in units of g cm$^{-3}$, mass $M$, radius $R$ and the surface gravity $g_s$ of the neutron stars used in our calculations.

| $\log \rho_c$ | $M$ ($M_\odot$) | $R$ (km) | $g_s$ ($10^{14}$ cm s$^{-2}$) |
|---|---|---|---|
| 14.60 | 0.75 | 13.17 | 0.63 |
| 14.97 | 1.40 | 12.92 | 1.35 |
| 15.22 | 2.01 | 11.18 | 3.11 |

respectively. Here, $\dot{M}$ is the mass-accretion rate, $s$ is the specific entropy, $t$ is the Schwarzschild time coordinate, and $\mu_i$ and $N_i$ are the chemical potential and number per unit mass of the $i$th elements, respectively. Equations (7) and (8) are called homologous and nonhomologous terms, respectively, where the former indicates homologous compression due to accretion, which causes compressional heating. We solve the above set of equations (1)–(6) numerically with the Henyey-type numerical scheme for the implicit method [25–27].

### 2.2. *Physics input*

There are various theoretical approaches to build the equation of state (EoS) of dense matter [32]. The cooling processes strongly depend on the EoS, especially at the core where hyperons, pion/kaon condensation, or quarks may appear. Different compositions correspond to different neutrino emission rates; as a result, by comparing theory with the observations of neutron star cooling, one can explore the properties of superdense matter in a neutron star. Since we mainly study the effect of shallow heating and compressional heating on the thermal state of transiently accreting neutron stars in the present work, we only adopt one EoS as used in our previous work [14]: we use the EoS constructed by Lattimer and Swesty (LS) with an incompressibility of 220 MeV [33] in the inner layers ($\rho \geq 10^{12.8}$ g cm$^{-3}$) and connect it to the EoSs in Refs. [34,35] for the outer layers ($\rho < 10^{12.8}$ g cm$^{-3}$). In addition, we include the effects of pion condensation [36], which makes the EoS softer; the baryon maximum mass of a neutron star is reduced from 2.53 to 2.21$M_\odot$. We adopt three representative NSs (0.75$M_\odot$, 1.4$M_\odot$, 2.01$M_\odot$) in our calculations, which can be seen in Table 1.

The thermal energy of an NS is lost from both the crust and the core primarily by neutrino emission. In the present work, neutrino emissions include the following processes: electron–positron pair, photo, and plasmon processes (see Eqs. (25)–(27) in Ref. [37]), the electron–ion bremsstrahlung process [38],

$$\varepsilon_\nu^{\rm brems.} = 3.8 \times 10^{19} \left(\frac{\rho}{\rho_{\rm nuc}}\right)^{1/3} T_9^8 \ {\rm erg\ cm^{-3}\ s^{-1}}, \tag{9}$$

the modified Urca (MURCA) process [39],

$$\varepsilon_\nu^{\rm MURCA} = 2.6 \times 10^{20} \left(\frac{\rho}{\rho_{\rm nuc}}\right)^{2/3} T_9^8 \ {\rm erg\ cm^{-3}\ s^{-1}}, \tag{10}$$

where $\rho_{\rm nuc}$ represents the nuclear density, and strong neutrino losses due to pion condensation (see Table 1 in Ref. [36]). For the neutrino emission rates due to pion condensation, we adopt the case $\tilde{g}' = 0.5$ (see Table 1 in Ref. [36]), which causes strong cooling. In addition, if superfluidity is involved, Cooper pair breaking and formation processes are considered (see Eqs. (31)–(33) in Ref. [40]).



Downloaded from https://academic.oup.com/ptep/article/2020/4/043E01/5823818 by guest on 16 August 2022

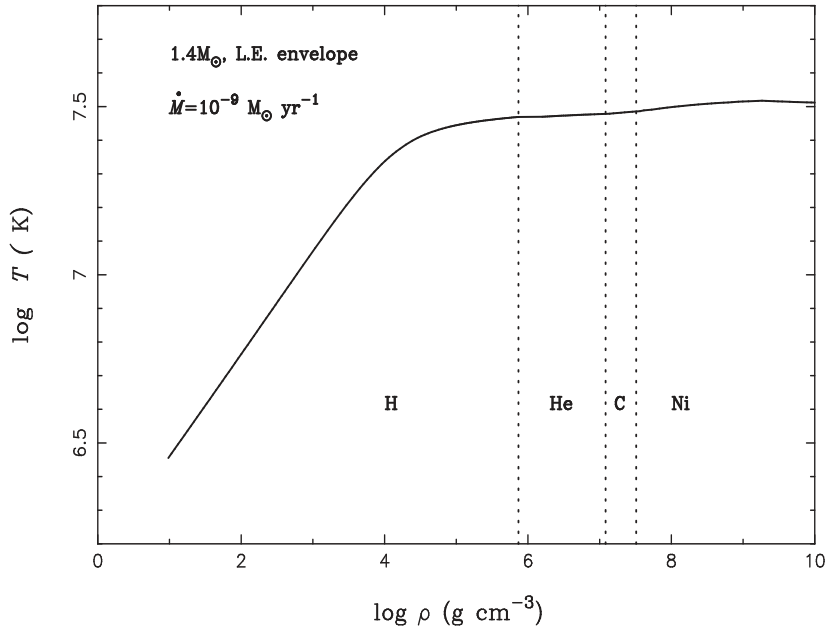


**Fig. 1.** Surface composition of light elements for a $1.4\mathrm{M}_{\odot}$ neutron star with $\dot{M} = 10^{-9}\ \mathrm{M}_{\odot}\ \mathrm{yr}^{-1}$. The dotted lines indicate the boundaries for these elements.

The deep crustal heating is given by [2–5]

$$Q_i = 6.03 \times \dot{M}_{-10}\, q_i\ 10^{33}\ \mathrm{erg\ s}^{-1}, \tag{11}$$

where $\dot{M}_{-10} = \frac{\dot{M}}{10^{-10}}$ is the mass-accretion rate in units of $\mathrm{M}_{\odot}\ \mathrm{yr}^{-1}$ and $q_i$ denotes the heat deposited in the $i$th reaction surface (see Tables 1 and 2 in Ref. [2]).

Based on Refs. [1,21,41], the energy released from shallow heating is proportional to the mass-accretion rate:

$$Q_{\mathrm{sh}-j} = 6.03 \times \dot{M}_{-10}\, q_{\mathrm{sh}}\ 10^{33}\ \mathrm{erg\ s}^{-1}, \tag{12}$$

where $q_{\mathrm{sh}}$ represents the heat deposited in the $j$th surface of the crust. As a result, the energy production rate from deep crustal heating and shallow heating can be evaluated from $Q_i/\Delta M_i$ and $Q_{\mathrm{sh}-j}/\Delta M_j$, respectively, where $\Delta M$ corresponds to the mass of the $i(j)$th reaction surface.

For the surface composition in the accretion layer, for simplicity, we assume two cases: heavy elements (Ni only) and light elements (Ni, C, He, and H). One can see a model for a $1.4\mathrm{M}_{\odot}$ NS with the surface composition of light elements (hereafter LE) in Fig. 1.

## 3. Quiescent luminosity of quasi-stationary SXTs

For the purpose of studying the effect of shallow heating/compressional heating on the thermal state of SXTs, we review the theoretical heating curves $L_{\gamma}^{\infty} - \langle\dot{M}\rangle$ first, where $L_{\gamma}^{\infty} = 4\pi\sigma\,(T_s)^4 R^2 (1 - r_g/R)$ is the photon surface luminosity as detected by a distant observer (also called "redshifted luminosity") and $T_s$ is the surface temperature, with $r_g = 2GM/c^2$ being the gravitational radius. Under the assumption of a constant mass-accretion rate $\dot{M}$, we perform an evolutionary calculation of accreting NSs with a constant accretion rate ($\langle\dot{M}\rangle \sim 10^{-13}$–$10^{-8}\ \mathrm{M}_{\odot}\ \mathrm{yr}^{-1}$) until the nonhomologous term of the gravitational energy vanishes ($\varepsilon_g^{(\mathrm{nh})} = 0$) [25]. In addition, in the previous studies of quasi-stationary SXTs, the energy generation only comes from deep crustal heating [7–9,13,15,17,21,42].



Downloaded from https://academic.oup.com/ptep/article/2020/4/043E01/5823818 by guest on 16 August 2022

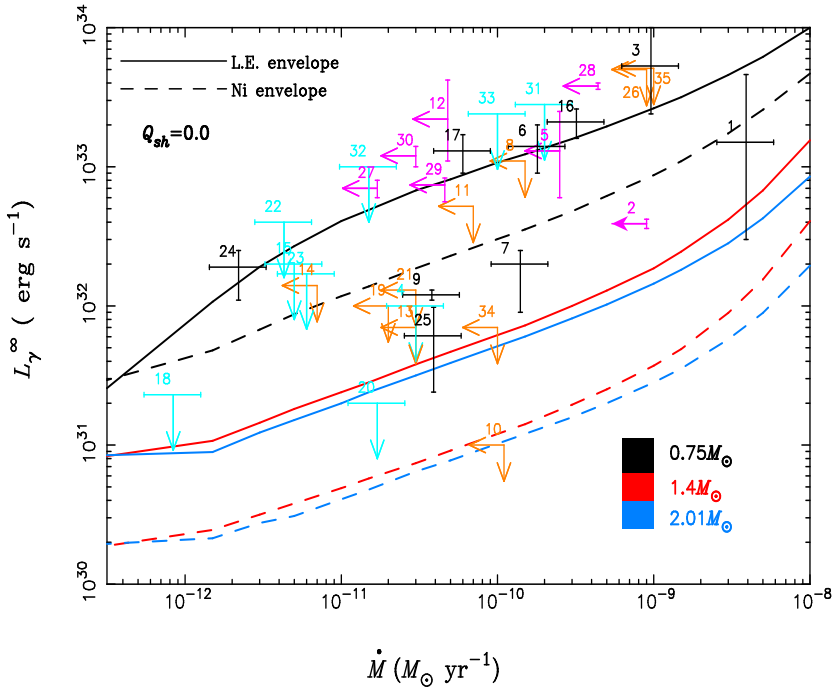


**Fig. 2.** Redshifted quiescent luminosity ($L_\gamma^\infty$) versus averaged mass-accretion rate ($\langle\dot{M}\rangle$) for different neutron star masses (marked by color) and surface compositions (marked by line style). The error bars and arrows show the observations of 35 SXTs collected in Ref. [15]. The numbers 1–35 correspond to the following source names: 1: 4U 2129+47, 2: KS 1731-260, 3: 4U1608-522, 4: Ter 5X-1, 5: 1M 1716-315, 6: XTE J1709, 7: MXB 1659-29, 8: XB 1732-304, 9: Cen X-4, 10: 1H 1905+00, 11: 2S 1803-245, 12: 4U 1730-22, 13: EXO 1747, 14: XTE 2123, 15: SAX J1810.8, 16: Aql X-1, 17: NGC 6440 X-1, 18: NGC 6440 X-2, 19: XTE J0929, 20: SAX J1808.4, 21: XTE J1807, 22: XTE J1751, 23: XTE J1814, 24: IGR J00291, 25: HETE J1900.1, 26: XTE J1701, 27: Ter 5X-2, 28: EXO 0748, 29: 1RXS J180408, 30: Ter 5 X-3, 31: SAX J1750.8, 32: Swift J1756.9, 33: GRS 1747, 34: IGR J18245, 35: MAXI J0556.

In order to be consistent with the previous studies, we do not include compressional heating ($\varepsilon_g^{(\mathrm{h})} = 0$), i.e., $\varepsilon_g = 0$. With the above physics input, but with the energy generation only including deep crustal heating, the heating curves are calculated and compared with the observations of 35 SXTs [15] in Fig. 2. One can see that the heating curves are unable to explain the whole range of observational samples, especially the hotter sources: 3: 4U1608-522, 26: XTE J1701, 35: MAXI J0556, 16: Aql X-1, 28: EXO 0748, 12: 4U 1730-22, 30: Ter 5 X-3, and 27: Ter 5X-2.

One way to fit the hotter sources is to include the superfluidity, as many authors have done [13,15]. Here, we want to show additional heating such as shallow heating/compressional heating, which may have a significant contribution to the equilibrium redshifted luminosities ($L_\gamma^\infty$).

## 4. The equilibrium state of transiently accreting NSs with additional heating

Yakovlev et al. studied thermal states of transiently accreting neutron stars determined by deep crustal heating with a simple toy model [7]. References [14,15] studied the same issue with more complicated evolutionary calculations. In this article, we study the thermal states of transiently accreting neutron stars determined by deep crustal heating in addition to shallow heating/compressional heating and see the effect of these crustal properties on the thermal states of SXTs. Although shallow heating occurs in the crustal cooling sources, it may affect the equilibrium state of these SXTs. In the study of crust cooling curves, one should switch accretion on, overheat the crust, then switch accretion off and



Downloaded from https://academic.oup.com/ptep/article/2020/4/043E01/5823818 by guest on 16 August 2022

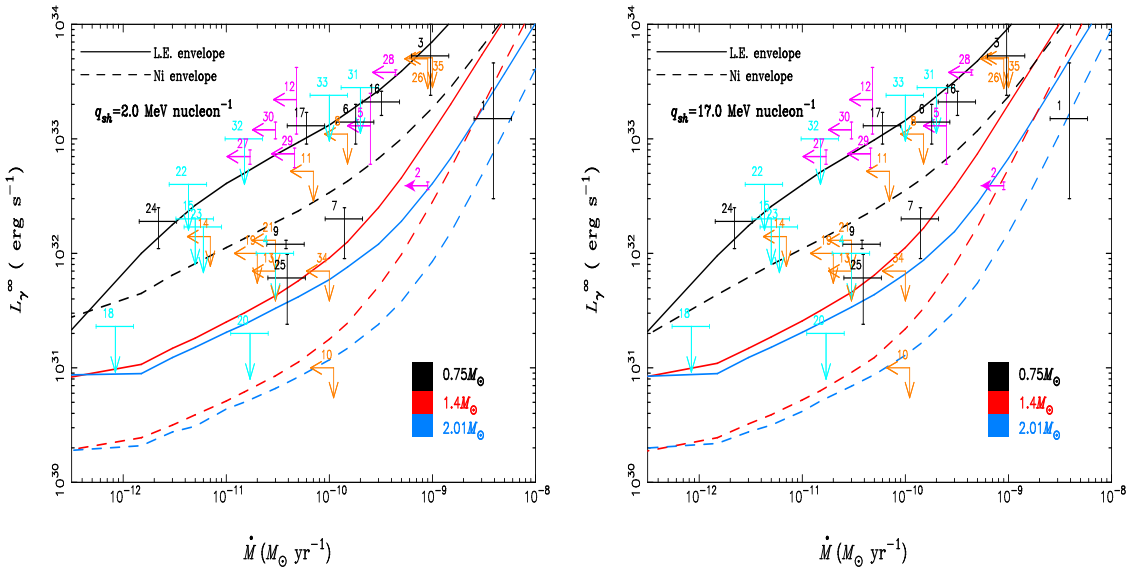


**Fig. 3.** The same as Fig. 2 but with shallow crustal heating deposited over the column depth ranging from $y_{\rm sh}/3$ to $y_{\rm sh} \times 3$, where $y = p/g$ is the column depth and $y_{\rm sh} = 6.5 \times 10^{13}$ g cm$^{-2}$. In the left panel, $q_{\rm sh} = 2.0$ MeV nucleon$^{-1}$; in the right panel, $q_{\rm sh} = 17.0$ MeV nucleon$^{-1}$.

model the subsequent crust–core relaxation [18,21,22], but for long-term evolutionary calculations, since the quiescence intervals are much shorter than the typical timescales of NS thermal relaxation ($\sim 10^4$ yr) [43], we can assume a constant accretion rate and neglect short-term variability in the NS crust [7]. Meanwhile, the accretion and quiescent duration are quite different for different sources. So, this will enable us to investigate the effect of crustal properties with a constant average accretion rate without studying the whole accretion outburst history. In the following, we explore the effect of shallow heating and compressional heating on the thermal state of transiently accreting NSs by assuming a constant accretion rate in our evolutionary calculations.

### *4.1. Equilibrium redshifted luminosities with shallow heating*

As the strength of the shallow heating is uncertain, it is inferred to be of the order $\sim$ 0–2 MeV nucleon$^{-1}$ [18,19,41,44–48], but one exceptional source, MAXI J0556-332, requires $\sim$ 6–17 MeV nucleon$^{-1}$ [20–22]. As a result, in our model, we set the values of shallow heating $q_{\rm sh}$ in the range $\sim$ 0–17 MeV nucleon$^{-1}$. Simultaneously, we assume that the shallow heating is uniformly deposited over the column depth $y_{\rm sh}/3 - y_{\rm sh} \times 3$ as inferred from the quiescent light curve of MAXI J0556-332 by Ref. [21], where $y = P/g$ is the column depth and $y_{\rm sh} = 6.5 \times 10^{13}$ g cm$^{-2}$.

By considering the energy generation from both deep crustal heating and shallow heating, the equilibrium redshifted luminosities are calculated. The results are shown in Fig. 3; we compare Fig. 3 with Fig. 2 and can see that shallow heating makes a significant contribution to the quiescent luminosity, especially at high accretion rates ($\dot{M} > 10^{-10}$ M$_\odot$ yr$^{-1}$). In order to see the effect of the strength of shallow heating, we show $q_{\rm sh} = 2.0$ MeV nucleon$^{-1}$ in the left panel and $q_{\rm sh} = 17.0$ MeV nucleon$^{-1}$ in the right panel; one can find that the larger the shallow heating, the more luminous the redshifted luminosity for a fixed accretion rate ($\dot{M} > 10^{-10}$ M$_\odot$ yr$^{-1}$). As a result, the hotter sources, 3: 4U 1608-522, 26: XTE J1701, 35: MAXI J0556, 28: EXO 0748, and 16: Aql X-1, can be explained well with shallow heating. However, the sources 12: 4U1730-22, 30: Ter 5X-3, and 27: Ter 5X-2 with accretion rates $\dot{M} \sim 10^{-11}$–$10^{-10}$ M$_\odot$ yr$^{-1}$ still cannot be explained, which



Downloaded from https://academic.oup.com/ptep/article/2020/4/043E01/5823818 by guest on 16 August 2022

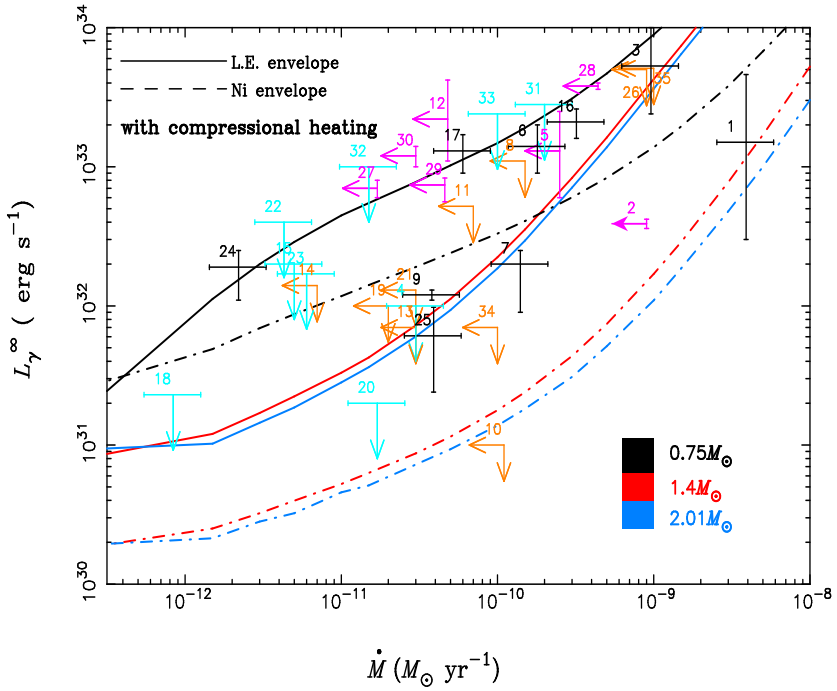


**Fig. 4.** The same as in Fig. 2 but with the energy generation due to both deep crustal heating and compressional heating.

indicates that superfluidity is still needed even if shallow heating is included. We also investigated the effect of shallow heating at different depths, but the depth of the shallow heating has a smaller effect on the equilibrium luminosity. Our results are consistent with Ref. [49], in which the authors calculate the effect of shallow heating by using the observed outburst behavior of Aql X-1; they also show that shallow heating contributes significantly to the equilibrium state.

### *4.2. Equilibrium redshifted luminosities with compressional heating*

Shallow heating is proposed to fit the crustal cooling curves, while Ref. [24] studied the crustal cooling curve of MAXI J0556-332 without shallow heating. They explained the light curve of MAXI J0556-332 by considering energy generation including deep crustal heating, compressional heating, and hot-CNO burning, as the hot-CNO cycle occurs in the envelope when $0.2 < T_9 < 0.5$ [50], where $T_9 = T/10^9$. In this section, we only explore the effect of compressional heating on the equilibrium redshifted luminosity. By considering energy generation coming from both deep crustal heating and compressional heating, the heating curves are shown in Fig. 4. By comparing Fig. 4 with Fig. 2, one can see that the compressional heating also makes a significant contribution to the equilibrium redshifted luminosity. For high accretion rates, the effect is very obvious, while, for low accretion rates, there is almost no effect on the equilibrium redshifted luminosity, which indicates that the effect of compressional heating is parallel to shallow heating. However, compressional heating only depends on the mass-accretion rate (see Eq. (7) for details) while shallow heating depends on both mass-accretion rate and shallow heating strength (see Eq. (12) for details). As a result, for a proper shallow heat $q_{\rm sh}$ and mass-accretion rate $\dot{M}$, the effect of shallow heating could be simulated by compressional heating ($\varepsilon_n^{(\rm h)}$).



Downloaded from https://academic.oup.com/ptep/article/2020/4/043E01/5823818 by guest on 16 August 2022

## 5. Discussions

In Sect. 4, we explored the effects of shallow heating and compressional heating on the equilibrium redshifted luminosities. Both of them make a significant contribution to the equilibrium state. As shallow heating has more parameters ($\langle\dot{M}\rangle, q_{\rm sh}$) than compressional heating, in this section, we discuss the effect of shallow heating in more detail. In order to obtain the details of the value of $q_{\rm sh}$ on the quiescent luminosity of a transiently accreting neutron star, we select one heating curve with different values of $q_{\rm sh}$ for analysis; the shallow heating is also deposited over the column depth $y_{\rm sh}/3 - y_{\rm sh} \times 3$, $y_{\rm sh} = 6.5 \times 10^{13}$ g cm$^{-2}$. As seen in Fig. 5, we calculated the equilibrium redshifted luminosity versus averaged mass-accretion rate with different shallow heating strengths ($q_{\rm sh} \sim 0 - 17$ MeV nucleon$^{-1}$) (coded by color) for a 1.4M$_\odot$ NS. One can see that the shallow heating has a significant contribution at high accretion rates ($\dot{M} > 10^{-10}$ M$_\odot$ yr$^{-1}$); for the medium accretion rates ($\dot{M} \sim 10^{-11}$–$10^{-10}$ M$_\odot$ yr$^{-1}$) the shallow heating only has a little effect, while for the low accretion rates ($\dot{M} \sim 10^{-13}$–$10^{-11}$ M$_\odot$ yr$^{-1}$) there is almost no effect on the equilibrium redshifted luminosity. This is why, in Fig. 3, the hotter sources, 3: 4U 1608-522, 26: XTE J1701, 35: MAXI J0556, 28: EXO 0748, and 16: Aql X-1, with high accretion rates can be explained well with shallow heating, but the sources 12: 4U1730-22, 30: Ter 5X-3, and 27: Ter 5X-2 with medium accretion rates still cannot be explained.

In addition, in the left panel of Fig. 6, we give the time evolution of redshifted luminosities for a 1.4M$_\odot$ neutron star with a surface composition of light elements and a mass-accretion rate of $\dot{M} = 10^{-9}$ M$_\odot$ yr$^{-1}$ until steady state with different values of $q_{\rm sh}$ (coded by color). This shows that shallow heating begins to take effect at $t > 10^6$ s; the redshifted luminosities at steady state ($t > 10^{11}$ s) are enhanced with increasing $q_{\rm sh}$ . In the right panel of Fig. 6, we plot the steady-state luminosities with different $q_{\rm sh}$ for 0.75M$_\odot$ and 1.4M$_\odot$ neutron stars. One can see clearly that the

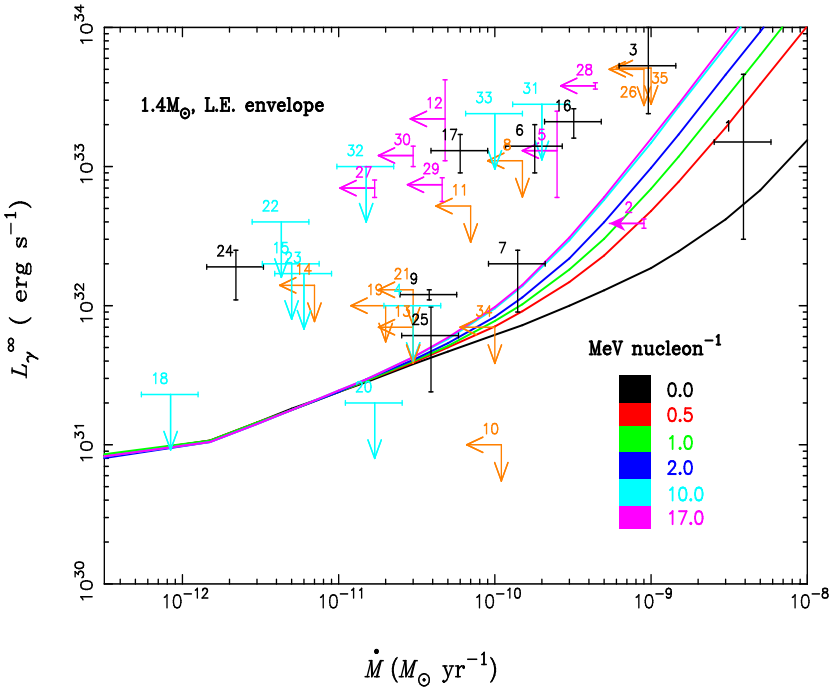


**Fig. 5.** Equilibrium redshifted luminosity versus averaged mass-accretion rate with different shallow heating strengths (marked by color) for a 1.4 M$_\odot$ neutron star with a light element envelope.



Downloaded from https://academic.oup.com/ptep/article/2020/4/043E01/5823818 by guest on 16 August 2022

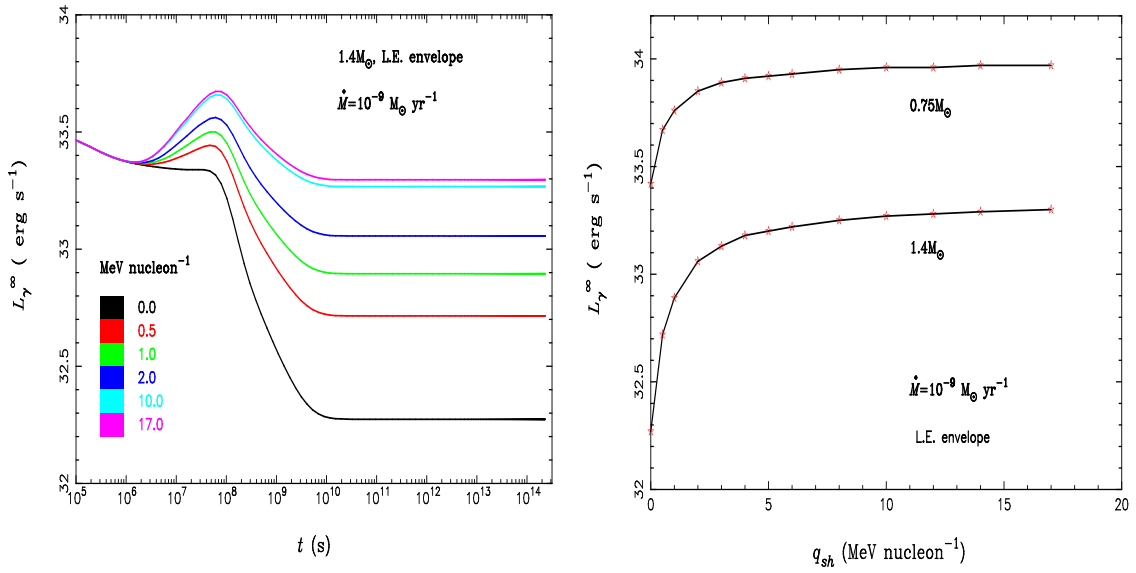


**Fig. 6.** Left: Time evolution of luminosities for a 1.4 $M_\odot$ neutron star with a light element envelope and mass-accretion rate $\dot{M} = 10^{-9}$ $M_\odot$ yr$^{-1}$ until steady state with different shallow heating values (coded by color). Right: Steady-state redshifted luminosities versus different values of $q_{\rm sh}$ for 0.75$M_\odot$ and 1.4$M_\odot$ neutron stars.

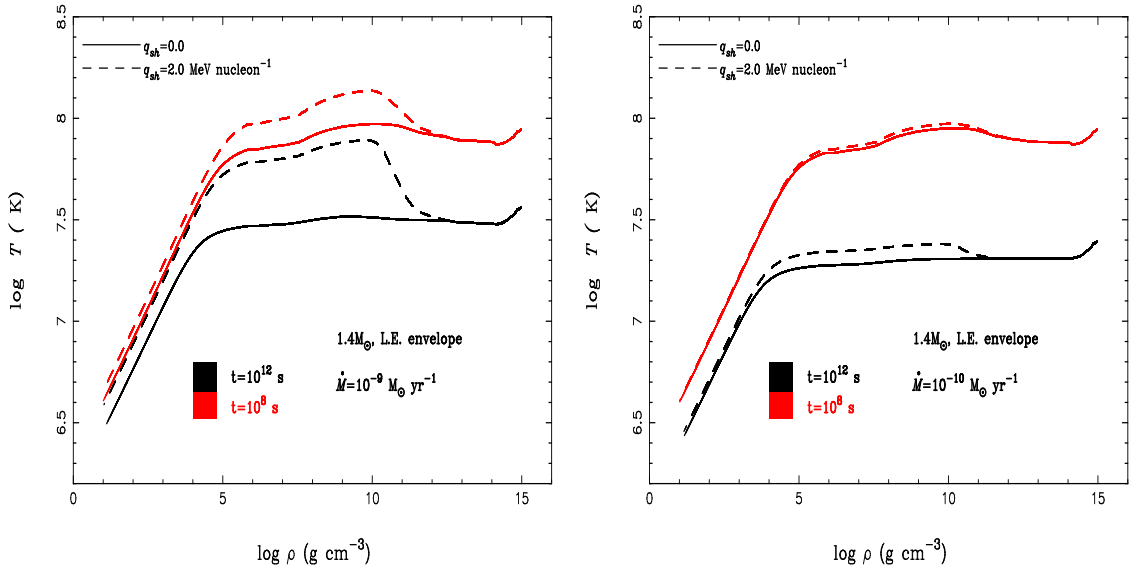


**Fig. 7.** Temperature of a 1.4 $M_\odot$ neutron star with a light element envelope versus density in the steady state ($t = 10^{12}$ s) and $t = 10^8$ s (marked by color); the solid lines represent $q_{\rm sh} = 0$ and the dashed lines represent the crustal heating $q_{\rm sh} = 2.0$ MeV nucleon$^{-1}$. Left: $\dot{M} = 10^{-9}$ $M_\odot$ yr$^{-1}$; right: $\dot{M} = 10^{-10}$ $M_\odot$ yr$^{-1}$.

equilibrium redshifted luminosity increases quickly when $q_{\rm sh} \lesssim 5$ MeV nucleon$^{-1}$; it is unchanged when $q_{\rm sh} > 5$ MeV nucleon$^{-1}$. Hence, we have very similar luminosities in Fig. 5 for $q_{\rm sh} = 10$ and 17 MeV nucleon$^{-1}$.

In Fig. 7 we illustrate the thermal structures for models of a 1.4$M_\odot$ neutron star with a surface composition of light elements. Notice that at $t = 10^8$ s the temperature is higher than the steady state ($t = 10^{12}$ s). These models have peak temperatures at densities $\rho \sim 10^6$–$10^{10}$ g cm$^{-3}$; these peaks are due to the shallow heating of Eq. 12. Meanwhile, the thermal structures displayed in the left ($\dot{M} = 10^{-9}$ $M_\odot$ yr$^{-1}$) and right ($\dot{M} = 10^{-10}$ $M_\odot$ yr$^{-1}$) panels of Fig. 7 show that the effect



Downloaded from https://academic.oup.com/ptep/article/2020/4/043E01/5823818 by guest on 16 August 2022

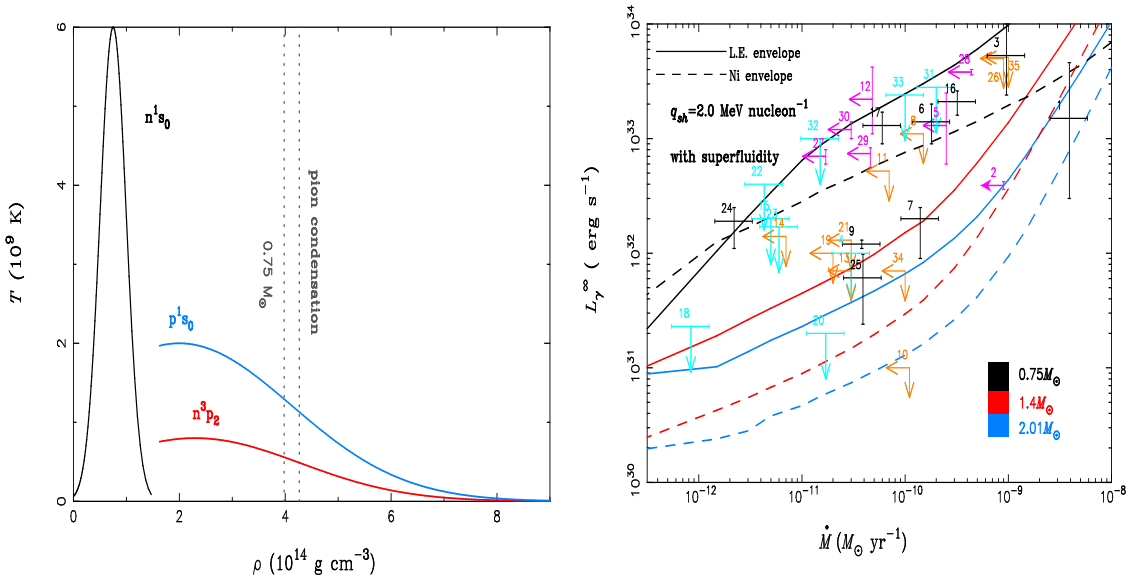


**Fig. 8.** Left: Critical temperature versus density. Dotted lines represent the threshold density of pion condensation and the central densities of 0.75$M_\odot$. Right: The same as in the left panel of Fig. 3 but with the effect of superfluidity.

of shallow heating is reduced as the mass-accretion rate decreases. So, it is easy to understand that shallow heating makes a significant contribution to the quiescent luminosities, especially for high accretion rates in Fig. 3.

Superfluidity is known to affect NS thermal evolution. Once matter becomes superfluid, neutrino emission must be suppressed due to the energy gap ($\Delta = \alpha T_{\rm cr}$) by a factor $\exp(-\Delta/T)$ [51,52], where $\alpha$ is a constant (1.76 for the $^1S_0$ state and 8.40 for the $^3P_2$ state) and $T_{\rm cr}$ is the critical temperature. In addition, a specific neutrino emission mechanism by Cooper pair breaking and formation (PBF) appears [40]. In order to explain the observations of the 35 SXTs with our model, based on the left panel of Fig. 3, which includes shallow heating together with deep crustal heating, we also include the effects of superfluidity in Fig. 8. In the left panel of Fig. 8 we show the density dependence of the critical temperature for $n^1s_0$, $n^3p_2$, $p^1s_0$. We fine-tuned the critical temperatures to fit the observations of quiescent luminosities. The heating curves with superfluidity displayed in the right panel of Fig. 8 show that the observations are perfectly fitted.

## 6. Closing remarks

In this paper, we studied thermal states of transiently accreting neutron stars with the effect of additional heating beyond deep crustal heating (cooling through neutrino emission and photon emission balanced by deep crustal heating in addition to shallow heating/compressional heating).

By considering that the energy generation comes from both deep and shallow heating/compressional heating with the use of evolutionary calculations, we investigated the equilibrium redshifted luminosity of transiently accreting neutron stars. Our results show that both shallow heating and compressional heating have significant effects on heating curves, especially at high mass-accretion rates ($\dot{M} > 10^{-10}$ $M_\odot$ yr$^{-1}$). By comparing our results with the 35 newest observations of SXTs, we found that the hotter sources, 3: 4U 1608-522, 26: XTE J1701, 35: MAXI J0556, 28: EXO 0748, and 16: Aql X-1, can be explained well with shallow heating/compressional heating. However, the sources 12: 4U1730-22, 30: Ter 5X-3, and 27: Ter 5X-2 with accretion rates



Downloaded from https://academic.oup.com/ptep/article/2020/4/043E01/5823818 by guest on 16 August 2022

$\dot{M} \sim 10^{-11}$–$10^{-10}$ $M_\odot$ yr$^{-1}$ still cannot be explained: superfluidity is still needed to explain the observations.

Thermal evolution analyses reveal that the effect of shallow heating does not operate when the accretion rate is small. For a fixed accretion rate ($\dot{M} > 10^{-10}\,M_\odot\,\mathrm{yr}^{-1}$), the value of the shallow heating has a significant effect when $q_{\rm sh} < 5$ MeV nucleon$^{-1}$. The equilibrium redshifted luminosities are almost the same when $q_{\rm sh} > 5$ MeV nucleon$^{-1}$.

For a proper shallow heat $q_{\rm sh}$ and mass-accretion rate $\dot{M}$, the effect of shallow heating could be simulated by compressional heating ($\varepsilon_n^{(\rm h)}$).

Finally, it is notable that shallow heating is an interesting topic in the study of SXTs. In addition, it will be very interesting if we use a much higher-level physics input (EoS, neutrino emission, and superfluidity) such as Refs. [15,18] in order to have a good view of the effect of shallow heating/compressional heating on the thermal state of SXTs. We leave these issues for future work.

**Acknowledgements**

We would like to thank the anonymous referee for the thorough review and very helpful comments. We also want to thank A. Dohi for useful discussions. This work has been supported by the National Natural Science Foundation of China under Nos. 11803026, 11473024, the XinJiang University Science Fund, the XinJiang Science Fund of 2017 Tianchi Program, and the XinJiang Science Fund for Distinguished Young Scholars under No. QN2016YX0049.

## References

[1] R. Wijnands, N. Degenaar, and D. Page, J. Astrophys. Astron. **38**, 49, (2017).
[2] P. Haensel and J. L. Zdunik, Astron. Astrophys. **227**, 431 (1990).
[3] P. Haensel and J. L. Zdunik, Astron. Astrophys. **404**, L33 (2003).
[4] P. Haensel and J. L. Zdunik, Astron. Astrophys. **480**, 459 (2008).
[5] E. F. Brown, L. Bildsten, and R. E. Rutledge, Astrophys. J. Lett. **504**, L95 (1998).
[6] G. Ushomirsky and R. E. Rutledge, Mon. Not. R. Astron. Soc. **325**, 1157 (2001).
[7] D. G. Yakovlev, K. P. Levenfish, and P. Haensel, Astron. Astrophys. **407**, 265 (2003).
[8] M. V. Beznogov and D. G. Yakovlev, Mon. Not. R. Astron. Soc. **447**, 1598 (2015).
[9] M. V. Beznogov and D. G. Yakovlev, Mon. Not. R. Astron. Soc. **452**, 540 (2015).
[10] C. O. Heinke, P. G. Jonker, R. Wijnands, and R. E. Taam, Astrophys. J. **660**, 1424 (2007).
[11] C. O. Heinke, P. G. Jonker, R. Wijnands, C. J. Deloye, and R. E. Taam, Astrophys. J. **691**, 1035 (2009).
[12] C. O. Heinke et al., Astrophys. J. **714**, 894 (2010).
[13] S. Han and A. W. Steiner, Phys. Rev. C **96**, 035802 (2017).
[14] Y. Matsuo, H. Liu, M.-a. Hashimoto, and T. Noda, Int. J. Mod. Phys. E **27**, 1850067 (2018).
[15] A. Y. Potekhin, A. I. Chugunov, and G. Chabrier, Astron. Astrophys. **629**, A88 (2019).
[16] Y. Zhao, C. O. Heinke, S. S. Tsygankov, W. C. G. Ho, A. Y. Potekhin, and A. W. Shaw, Mon. Not. R. Astron. Soc. **488**, 4427 (2019).
[17] E. F. Brown and A. Cumming, Astrophys. J. **698**, 1020 (2009).
[18] L. S. Ootes, R. Wijnands, D. Page, and N. Degenaar, Mon. Not. R. Astron. Soc. **477**, 2900 (2018).
[19] A. Y. Potekhin, A. I. Chugunov, and G. Chabrier, Astron. Astrophys. **629**, A88 (2019).
[20] J. Homan, J. K. Fridriksson, R. Wijnands, E. M. Cackett, N. Degenaar, M. Linares, D. Lin, and R. A. Remillard, Astrophys. J. **795**, 131 (2014).
[21] A. Deibel, A. Cumming, E. F. Brown, and D. Page, Astrophys. J. Lett. **809**, L31 (2015).
[22] A. S. Parikh et al., Astrophys. J. Lett. **851**, L28 (2017).
[23] A. C. Waterhouse, N. Degenaar, R. Wijnands, E. F. Brown, J. M. Miller, D. Altamirano, and M. Linares, Mon. Not. R. Astron. Soc. **456**, 4001 (2016).
[24] H. Liu, Y. Matsuo, M.-A. Hashimoto, T. Noda, and M. Y. Fujimoto, J. Phys. Soc. Jpn. **86**, 123901 (2017).
[25] M. Y. Fujimoto, T. Hanawa, I. Iben Jr, and M. B. Richardson, Astrophys. J. **278**, 813 (1984).
[26] D. Sugimoto, Astrophys. J. **159**, 619 (1970).
[27] T. Hanawa and M. Y. Fujimoto, Publ. Astron. Soc. Jpn. **36**, 199 (1984).



Downloaded from https://academic.oup.com/ptep/article/2020/4/043E01/5823818 by guest on 16 August 2022

[28] K. S. Thorne, Astrophys. J. **212**, 825 (1977).
[29] D. A. Baiko, P. Haensel, and D. G. Yakovlev, Astron. Astrophys. **374**, 151 (2001).
[30] A. Y. Potekhin, J. A. Pons, and D. Page, Space Sci. Rev. **191**, 239 (2015).
[31] D. Sugimoto, K. Nomoto, and Y. Eriguchi, Prog. Theor. Phys. Suppl. **70**, 115 (1981).
[32] M. Oertel, M. Hempel, T. Klähn, and S. Typel, Rev. Mod. Phys. **89**, 015007 (2017).
[33] J. M. Lattimer and F. D. Swesty, Nucl. Phys. A **535**, 331 (1991).
[34] G. Baym, C. Pethick, and P. Sutherland, Astrophys. J. **170**, 299 (1971).
[35] M. B. Richardson, H. M. van Horn, K. F. Ratcliff, and R. C. Malone, Astrophys. J. **255**, 624 (1982).
[36] H. Umeda, K. Nomoto, S. Tsuruta, T. Muto, and T. Tatsumi, Astrophys. J. **431**, 309 (1994).
[37] G. Beaudet, V. Petrosian, and E. E. Salpeter, Astrophys. J. **150**, 979 (1967).
[38] G. G. Festa and M. A. Ruderman, Phys. Rev. **180**, 1227 (1969).
[39] B. L. Friman and O. V. Maxwell, Astrophys. J. **232**, 541 (1979).
[40] D. Page, J. M. Lattimer, M. Prakash, and A. W. Steiner, Astrophys. J. Suppl. **155**, 623 (2004).
[41] N. Degenaar, L. S. Ootes, D. Page, R. Wijnands, A. S. Parikh, J. Homan, E. M. Cackett, J. M. Miller, D. Altamirano, and M. Linares, Mon. Not. R. Astron. Soc. **488**, 4477 (2019).
[42] M. Fortin, G. Taranto, G. F. Burgio, P. Haensel, H.-J. Schulze, and J. L. Zdunik, Mon. Not. R. Astron. Soc. **475**, 5010 (2018).
[43] M. Colpi, U. Geppert, D. Page, and A. Possenti, Astrophys. J. Lett. **548**, L175 (2001).
[44] N. Degenaar, E. F. Brown, and R. Wijnands, Mon. Not. R. Astron. Soc. **418**, L152 (2011).
[45] N. Degenaar, Z. Medin, A. Cumming, R. Wijnands, M. T. Wolff, E. M. Cackett, J. M. Miller, P. G. Jonker, J. Homan, and E. F. Brown, Astrophys. J. **791**, 47 (2014).
[46] N. Degenaar et al., Mon. Not. R. Astron. Soc. **451**, 2071 (2015).
[47] D. Page and S. Reddy, Phys. Rev. Lett. **111**, 241102 (2013).
[48] A. S. Parikh et al., Mon. Not. R. Astron. Soc. **466**, 4074 (2017).
[49] L. S. Ootes, R. Wijnands, and D. Page, Astron. Astrophys. **630**, A95 (2019).
[50] R. K. Wallace and S. E. Woosley, Astrophys. J. Suppl. **45**, 389 (1981).
[51] S. Tsuruta, Phys. Rept. **292**, 1 (1998).
[52] S. Tsuruta, J. Sadino, and A. Kobelski, Astrophys. J. **691**, 621 (2009).

Downloaded from https://academic.oup.com/ptep/article/2020/4/043E01/5823818 by guest on 16 August 2022